International Journal of Mechanical and Electrical Engineering
ISSN: 3005-9615 (Print), ISSN: 3005-7132 (Online) | Volume 8, Number 3, Year 2026
DOI: https://doi.org/10.62051/ijmee.v8n3.09
Journal homepage: https://wepub.org/index.php/IJMEE/index

Mechanism of Casing Ovality Deformation in Deep Shale Gas Wells during Hydraulic Fracturing

Pan Fang [1, 2, *], Maojun Li [1, 2], Haibo Zheng [3], Yutian Han [4], Hui Feng [4], Yongjun Hou [1, 2]

[1] School of Mechanical Engineering, Southwest Petroleum University, Chengdu Sichuan, 610500, China

[2] Oil and Gas Equipment Technology Sharing and Service Platform of Sichuan Province, Southwest Petroleum University, Chengdu Sichuan, 610500, China

[3] Sichuan Tianshi Hechuang Technology Co., Ltd., Chengdu Sichuan, 610500, China

[4] Petrochina Tarim Oilfield Company, Korla, Xinjiang, 841000, China

* Corresponding author: Pan Fang

ABSTRACT

Casing deformation is a major constraint in the efficient development of shale gas horizontal wells during hydraulic fracturing. This study investigates the deformation characteristics and influencing factors in shale gas wells of the Zigong block. A finite element model of the shale–cement sheath–casing system for deep shale gas wells was established based on shale swelling mechanics. Through numerical simulations, the mechanism of casing deformation induced by shale swelling during hydraulic fracturing was determined, and the casing deformation patterns under the combined effects of shale swelling and cementing quality were revealed. Results show that shale swelling significantly increases casing compressive stress and can induce severe deformation. The casing stress distribution along the wellbore axis is strongly affected by the extent of shale hydration. In addition, cement sheath voids and elliptical geometry significantly affect casing stress. Elliptical cement sheaths exacerbate casing elliptical deformation, while cement sheath voids cause localized outward bulging of the casing. The orientation of cementing defects influences the casing's stress and deformation extent. Based on these findings, targeted strategies are proposed to mitigate deformation risks. This study provides new insights into casing failure mechanisms and offers theoretical guidance for fracture design and well integrity management in shale gas reservoirs.

KEYWORDS

Shale Gas Reservoirs; Casing Deformation; Shale Swelling; Cementing Quality; Compressive Deformation.

1. INTRODUCTION

In recent years, China’s shale gas industry has experienced rapid growth, particularly in the Sichuan Basin. Multistage hydraulic fracturing plays a critical role in enabling large-scale development and has driven significant production increases. However, due to the complex geological conditions in the Sichuan Basin [1]-[2], casing deformation has frequently occurred during hydraulic fracturing operations. According to statistics, as of December 2022, a total of 503 horizontal wells had undergone hydraulic fracturing in the Luzhou and Changning-Weiyuan blocks operated by PetroChina, and the Weirong block operated by Sinopec, among which 163 wells exhibited casing deformation. The deformation rates were 51.2%, 20.5%, and 42.2%, respectively [3]. These deformations not only cause operational risks, such as difficulties in deploying perforating guns and

bridge plug setting failures but also lead to non-uniform reservoir stimulation and fracturing stage inefficiencies, severely limiting the development of shale gas extraction. Consequently, systematic investigation into the mechanisms of casing deformation during shale gas fracturing is essential for enhancing wellbore integrity and guiding engineering design.

Current research on the mechanisms of casing deformation during fracturing primarily focuses on shear and compressive failure modes. For shear deformation, many scholars have found that slip along discontinuities such as fractures and faults during hydraulic fracturing is a key cause [4]-[8]. Yan et al. [9] demonstrated that high fracture pressures and temperature drops can create large internal-external pressure differentials, increasing the risk of casing shear deformation. Xi et al. [10] observed that when casing deformation is often influenced by abrupt mechanical property changes at lithological interfaces. Zhanghua Lian [11] pointed out that during volumetric fracturing, stress depletion in the zero-stress and tensile stress zones causes the cluster perforation casing of horizontal wells "hanging" in the formation, leading to significant flexural deformation and axial S-shaped deformation. Hao Yu [12] emphasized that casing failure results from a combination of factors, including decreased formation rock strength, asymmetric treatment zones, high operational pressures, and the redistribution of the in-situ stress field. For compressive deformation, Zhang et al. [13] identified sharp well trajectory changes as the main trigger, with cementing defects as contributing factors. Liu et al. [14] determined that fracturing fluid entering fractured shale can induce formation slippage and casing compressive. Yin et al. [15] developed a shale compression model showing that fracturing fluid mobilizes shale blocks, imposing asymmetric loads that induce elliptical casing deformation. Skomedal et al. [16] demonstrated through simulation that anisotropic stress can lead to shear-induced casing ellipticity.

Some scholars have explained shear and compressive casing deformation mechanisms from engineering and geological perspectives. However, field observations show that post-fracturing casing deformation often appears as ovalization rather than shear failure in sections with underdeveloped faults and fractures, highlighting the need to investigate alternative deformation mechanisms. Recent research has increasingly focused on shale hydration induced by fluid invasion. Liu et al. [17] revealed that hydration causes clay mineral swelling, which intensifies over time. Wang et al. [18] observed that higher clay content increases water-shale interaction and structural damage, while hydration-induced stress stabilizes after an initial rise. Li et al. [19] observed that fluid-shale interactions caused formation damage, micro-fracture propagation, and swelling deformation, with the extent of deformation positively correlated with confining pressure and exposure duration. Gao et al. [20] demonstrated that the hydration process is accompanied by significant shale swelling, and the swelling magnitude increases with fracture complexity. Meng et al. [21] further indicated that crack density enhances water uptake, and Li et al. [22] reported that such swelling imposes mechanical loads sufficient to deform casing. These findings highlight the critical role of shale-fluid interactions in deformation. Additionally, low strength and high swelling potential of shale frequently compromise cementing quality, ultimately impairing casing integrity. Extensive previous studies [23]-[25] have investigated the relationship between cementing quality and casing deformation, focusing on bonding quality at cement-to-formation and cement-to-casing interfaces, and cement sheath geometry. These studies suggested that compromised cementing quality exacerbates stress concentration within the casing-cement system, ultimately inducing deformation, fluid leakage, or structural failure. Therefore, the impact of cementing quality in the fractured section should also be integrated into casing deformation analysis.

In summary, current research predominantly focuses on the evaluation of macroscopic geological factors, lacking systematic analysis of the cross-scale coupling mechanisms linking shale hydration-swelling, stress transfer, and casing deformation. Therefore, to address the issue of casing deformation in the southern Sichuan shale gas wells, this study establishes finite element models based on shale swelling mechanical. This study quantitatively analyzes the influence of shale swelling on casing stress distribution and evaluates the combined effects of shale swelling and cementing

defects. It also offers practical guidance for optimizing casing design and mitigating engineering risks in shale gas development.

2. CHARACTERISTICS AND CAUSATIVE ANALYSIS OF CASING DEFORMATION

In the Z201H54-2 well, for instance, the production casing employed was of steel grade TP140V, which exhibits excellent mechanical properties. Post-fracturing logging identified seven severe and four minor casing deformation points distributed along the 5247-5667 m interval, as shown in Figure 1. Microseismic events from this well indicated a zone of significant fracture development at 5580–5667 m.

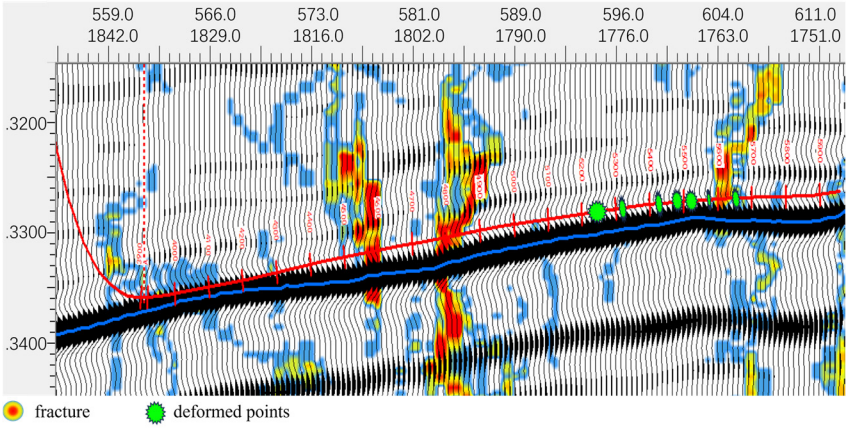

Fig 1. Measurement results of seismic events and deformation points of Z201H54-2 well

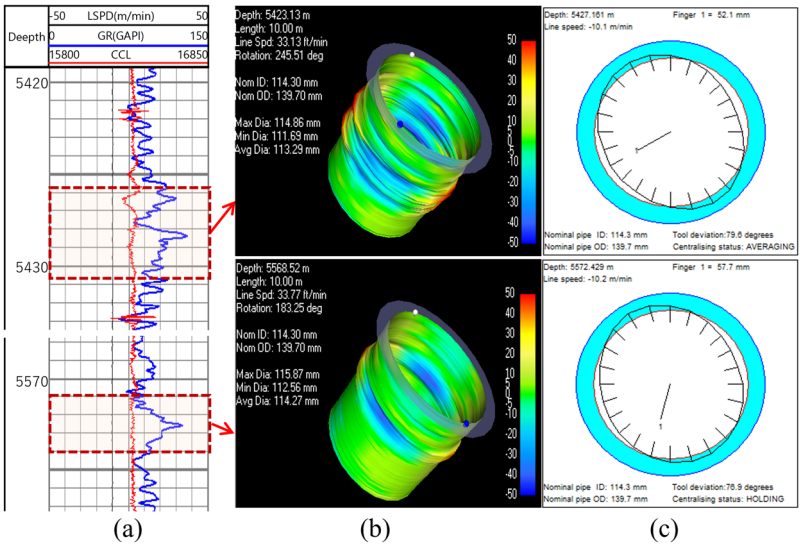

Fig 2. Reservoir section casing deformation and logging image interpretation of Z201H54-2 well: (a) Gamma ray log; (b) 3D view of compressive elliptical casing deformation; (c) Deformation cross-section

However, only one deformation point was found near this highly fractured zone. Consequently, it is preliminarily inferred that the probability of casing deformation caused by fracturing-induced formation slippage in this well is low. Further analysis revealed that all nine deformation points exhibited higher-than-average gamma ray (GR) logging values, as shown in the GR and multi-arm caliper logs in Figure 2(a). This observation implies elevated clay mineral content in the shale at these

locations, and hence a higher potential for hydration-induced swelling. Unlike the shear displacement deformation characteristics induced by fracture and fault slip, the casing in well Z201H54-2 exhibits a symmetric elliptical deformation caused by uniform compression, as shown in Figure 2(b) and Figure 2(b). In the figure, green represents the normal casing section, blue represents the casing shrinkage zone, and red represents the casing expansion zone. The standard internal casing diameter is 114.3 mm, with casing deformation points observed at a depth of 5430 m. The minimum and maximum internal diameters of the casing are 112.56 mm and 115.87 mm, respectively. Additionally, 25.4% of the wellbore interval in Z201H54-2 well exhibits poor cement bonding quality. Except for a single point, all casing deformation points were localized within the 5233–5667 m interval. Consequently, the influence of cementing quality on casing deformation in fractured intervals necessitates further investigation.

3. SHALE-CEMENT SHEATH-CASING COUPLED MECHANICAL MODEL

3.1. Finite Element Model of Shale-Cement Sheath-Casing System

In studies concerning the swelling behavior of Longmaxi Formation shale in the Sichuan Basin, several researchers have experimentally determined its swelling percentages. Z. Li et al. [26], G. Li et al. [27], and H. Li et al. [28] observed a swelling percentage of approximately 0.45% after 24 hours of immersion. Li et al. [19] further conducted swelling tests under confining pressure conditions and found that under a liquid pressure of 50 MPa, the shale strain remained below 0.7% after 30 hours of immersion, suggesting that high-pressure environments are more likely to promote shale swelling. During shale swelling deformation, high swelling-induced stresses are generated and act on the casing, thereby altering the external loading conditions of the casing. The influence of rock strain on the stress field is described by Eq. (1) [29]:

$$\sigma_{ij} = E\varepsilon_{ij} + \left(K - \frac{2E}{3}\right)\varepsilon_{\mathrm{v}} \tag{1}$$

Where σ_{ij} denotes the stress components in each direction induced by rock deformation, E is the elastic modulus, K is the bulk modulus, ε_{ij} represents the strain components in each direction, and ε_v is the volumetric strain.

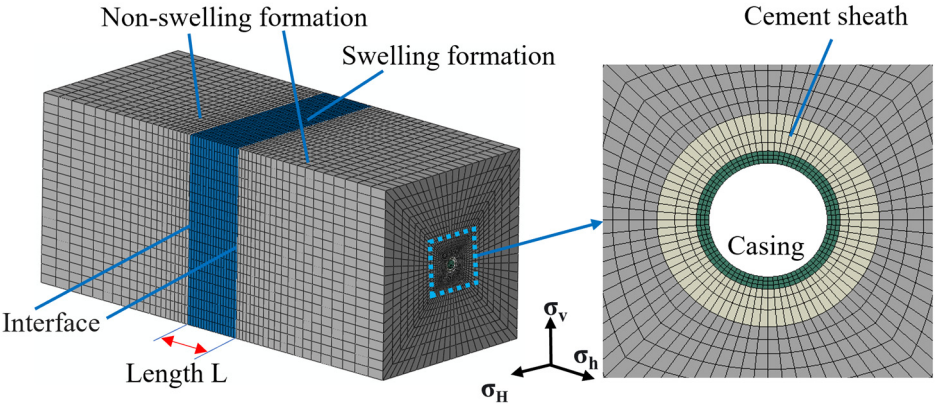

Fig 3. Finite element model of casing compressive caused by shale swelling

Due to the nonuniform distribution of fracturing fluids in the shale post-fracturing and the variable water sensitivity of shales with different clay contents, the degree of swelling in shale can vary significantly. Based on the morphological characteristics of casing deformation and the hypothesis of bulk shale swelling, a three-dimensional finite element model of the shale-cement sheath-casing system was developed, as shown in Figure 3. Post-fracturing retention of significant fracturing fluid volumes within the reservoir leads to heightened shale hydration. To simulate the influence of shale–

fluid interactions on casing behavior, the model was configured such that the two outer layers consisted of non-swelling bedrock, while the central layer represented a swelling shale zone with swelling percentages of 0%, 0.1%, 0.2%, 0.3%, and 0.4%. Considering that perforation clusters are oriented perpendicular to the wellbore trajectory, the angle between the swelling shale layer and the wellbore in the model was fixed at 90°. The overall model dimensions were 3 m × 3 m × 7 m, with the swelling shale layer having a length of 1 m. According to Saint-Venant theory, boundary effects on the wellbore were considered negligible as the formation size exceeds 10 times the wellbore diameter. The model was discretized using structured and variable-density meshing techniques to improve computation efficiency and convergence stability.

All model parameters were derived from field data acquired from horizontal wells in Zigong field, Sichuan Basin. Relevant parameters are tabulated in Table 1. The casing at the deformation-prone intervals was modeled using TP140V steel grade casing. The casing material was modeled using the von Mises yield criterion with a yield strength of 965 MPa. According to the von Mises criterion[30], the equivalent stress can be expressed as:

$$\sigma_e = \sqrt{\frac{1}{2}\left[(\sigma_1-\sigma_2)^2+(\sigma_2-\sigma_3)^2+(\sigma_3-\sigma_1)^2\right]} \tag{2}$$

where σ_1, σ_2, and σ_3 are the principal stresses of the casing in the three directions.

Table 1. Parameters of simulation model

Name	Non-swelling shale	Swelling shale	Cement sheath	Casing
Elastic modulus (GPa)	35	35	6	210
Poisson's ratio	0.25	0.25	0.18	0.2
Internal friction angle(°)	32	32	23	/
Cohesion (MPa)	16	16	12	/
Inner diameter (mm)	215.9	215.9	139.7	114.3
Swelling percentage (%)	/	0.1,0.2,0.3,0.4	/	/

3.2. Boundary Conditions

In the in-situ state, the rock mass is subjected to overburden pressure and horizontal principal stresses and remains in mechanical equilibrium. During hydraulic fracturing, stress states near stimulated zones become reconfigured, and casing and cement sheath jointly resist against shale deformation. The initial in-situ stress field was assigned using predefined field variables, with the maximum horizontal stress σ_H, minimum horizontal stress σ_h, and vertical stress σ_z set to 80 MPa, 73.6 MPa, and 94 MPa, respectively. Surface-to-surface contact defined interactions between swelling and non-swelling shale regions. The simulation of casing behavior under shale swelling was executed in three sequential steps. First, geostatic equilibrium was achieved without casing and cement elements, simulating a stress-rich, strain-neutral subsurface condition. Second, the rock in the wellbore region was deactivated using element-kill techniques, followed by reactivation of casing and cement elements. Drilling fluid pressure of 76.3 MPa was then applied to replicate post-cementing mechanical state. Finally, differential swelling percentages were assigned to the central shale layer to simulate compressive deformation of the casing caused by shale hydration during fracturing operations.

4. RESULTS AND DISCUSSION

The stress calculation results shown in Figure 4 indicate that no pronounced deformation occurs in the casing within the non-swelling zone. In contrast, stress concentration develops in the casing under

the compressive action of the swelling shale, resulting in an elliptical deformation pattern. This behavior is consistent with the findings reported by Fei Yin [15], and the deformation characteristics also agree well with the morphology observed in the 3D caliper logging results. Casing deformation is closely associated with the bedding distribution of the surrounding shale. When the bedding planes are oriented parallel to the wellbore axis, invasion of fracturing fluid causes shale swelling predominantly in the direction perpendicular to the bedding. Figure 5 further illustrates the contact stress distribution on the outer wall of the casing. As shale swelling increases, the induced swelling stress is transmitted to the casing through the cement sheath, leading to inward contraction of the casing in the direction of the vertical stress (σ_v), manifested as diameter reduction. Meanwhile, outward expansion occurs on both sides along the maximum horizontal stress direction (σ_H), where the casing continues to compress the surrounding shale, resulting in a significant increase in contact stress in this direction.

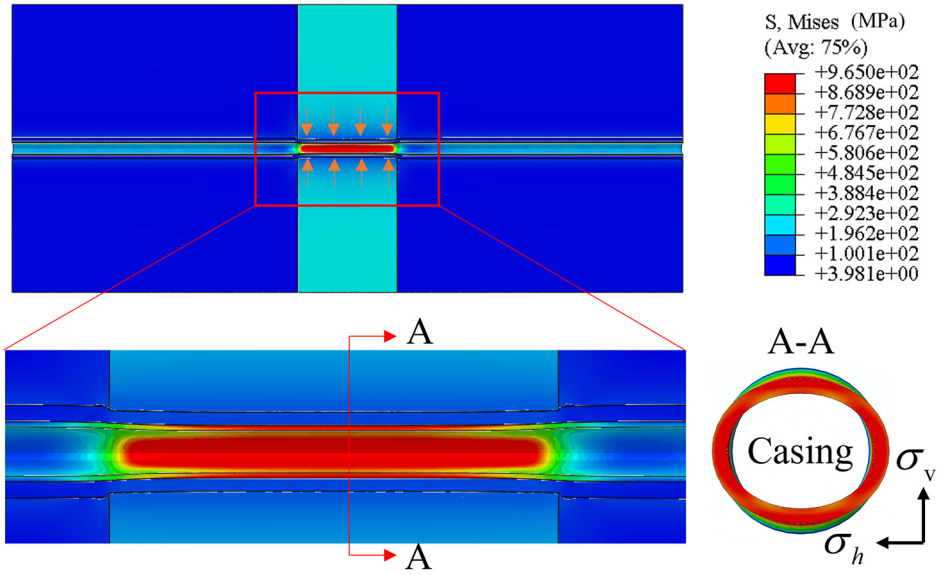

Fig 4. Stress distribution of shale gas well

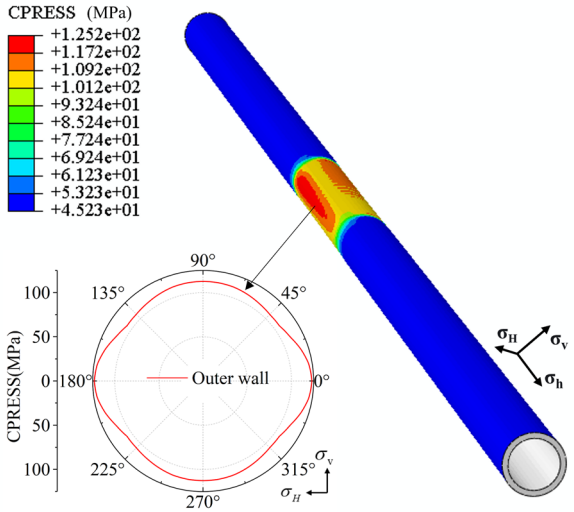

Fig 5. Contact stress distribution on the casing.

4.1. Influence of Shale Swelling on Casing Integrity

4.1.1. Influence of Shale Swelling Percentage on Casing Stress

Figure 6 presents the casing stress distributions under different shale swelling percentages. Under the initial in-situ stress condition (*SW*=0%), the casing stress remains relatively low. As the swelling percentage increases, casing stress rises progressively. When the swelling percentage reaches approximately 0.3%, the stress approaches the yield limit, indicating that the casing can no longer effectively resist the non-uniform compressive loading induced by formation swelling and deformation initiates. At a swelling percentage of 0.4%, the yielding zone expands rapidly. Figure 7 shows the variation in casing inner diameter within the swelling zone, where the dashed line denotes the nominal inner diameter. With increasing swelling percentage, casing ovalization becomes increasingly pronounced. To further elucidate the deformation mechanism during shale swelling, the change in casing inner diameter obtained from numerical simulations was extracted and converted into casing diameter reduction, as illustrated in Figure 8. The results indicate that the casing diameter reduction increases monotonically with shale swelling along the σ_v direction, reaching approximately 1.5 mm at a swelling percentage of 0.4%, which is in good agreement with the logging measurements shown in Figure 2. These findings demonstrate that shale swelling induced by fluid exposure can significantly compromise casing integrity. Therefore, shale swelling effects must be explicitly considered in the engineering design and hydraulic fracturing planning of shale gas horizontal wells.

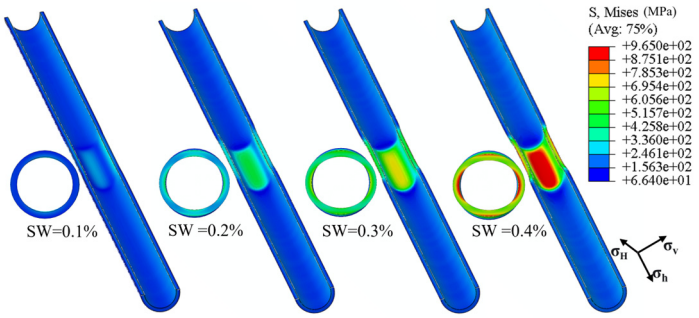

Fig 6. Contour plots of casing stress induced by shale swelling

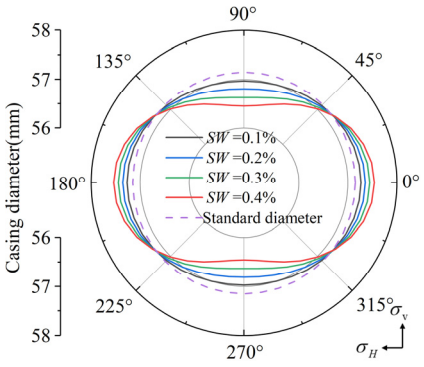

Fig 7. Casing inner diameter under different shale swelling percentages

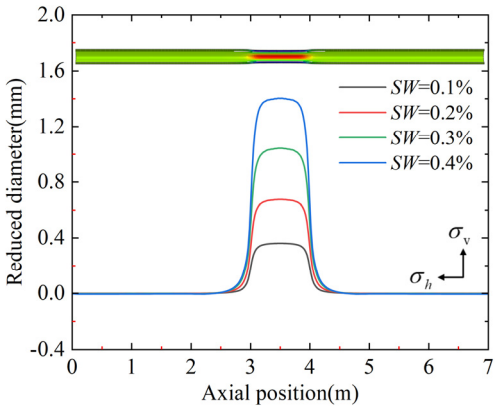

Fig 8. Casing diameter reduction along the wellbore axis

4.1.2. Influence of Shale Hydration Length on Casing Deformation

Volumetric hydraulic fracturing is widely applied to promote extensive fracture network propagation within target reservoirs, thereby providing effective flow pathways and enhancing overall reservoir conductivity. Owing to the inherent water absorption capacity of shale and the variability in fracture network development, the degree of reservoir hydration exhibits pronounced spatial heterogeneity. To elucidate the influence of shale hydration extent on the axial distribution of casing deformation, casing diameter reduction was simulated at a swelling percentage of 0.4% for hydration thicknesses of L=200mm, 400mm, 1200mm, and 2000mm, as shown in Figure 9. The results indicate that as the length of the hydrated interval increases, the axial range over which casing diameter reduction varies gradually expands and subsequently stabilizes at approximately 0.5 m. Specifically, the casing diameter reduction increases rapidly at first, followed by a progressively decreasing growth rate. Once stabilized, the diameter reduction within the hydrated zone remains at approximately 1.5 mm, which is consistent with field-measured logging data. This behavior provides a reasonable explanation for the observed phenomenon in which casing deformation magnitude remains similar while the deformation interval length varies. This response arises because the shale swelling ratio within the hydrated zone remains relatively uniform, whereas friction at the interface between hydrated and non-hydrated shale inhibits further expansion near the boundary. When the hydration thickness is relatively small (L=100 mm), the casing diameter reduction is limited to approximately 1.0 mm. In this case, the restrained swelling volume, combined with interfacial friction and the post-swelling strength degradation of shale, results in insufficient compressive force acting on the casing, leading to a smaller diameter reduction.

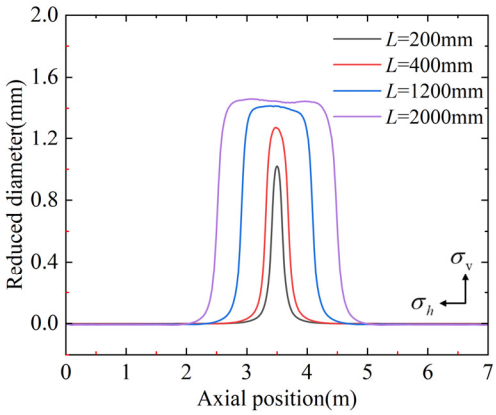

Fig 9. Casing diameter reduction at different hydration lengths

4.2. Influence of Shale Swelling and Cementing Quality on Casing Deformation

Cementing quality is essential for maintaining wellbore integrity and long-term stability in oil and gas wells. Key evaluation parameters include the bonding quality at the casing-to-cement and cement-to-formation interfaces and cement sheath ellipticity. However, in practical engineering scenarios such as shale reservoirs, maintaining high cementing quality remains challenging. Due to the low strength of shale formations, wellbore instability may occur during drilling as a result of drilling fluid invasion and drill string impact on the borehole wall [31], often leading to irregular cement sheath geometries after cementing. In addition, low displacement efficiency and flow disturbances during cement slurry placement can cause localized voids. Therefore, a series of models was established to systematically investigate the combined effects of key cementing quality factors and shale swelling on casing mechanical behavior.

4.2.1. Influence of Shale Swelling and Cement Sheath Ellipticity on Casing Deformation

The model shown in Figure 10 was employed to simulate the casing stress response for cement sheath ellipticities ranging from 1.0 to 1.5. In the model, a and b denote the lengths of the minor and major

axes of the elliptical cement sheath, respectively, and the ellipticity is defined as $\varepsilon = b/a$. The azimuth angle α is defined as the angle between the major axis of the cement sheath and the direction of the maximum horizontal in-situ stress. In addition, the maximum casing stress was calculated for different orientations of the major axis of the elliptical cement sheath to elucidate its influence on casing deformation in shale gas wells. Owing to the symmetry of the boundary conditions, only azimuthal angles ranging from 0° to 90° were considered in this study.

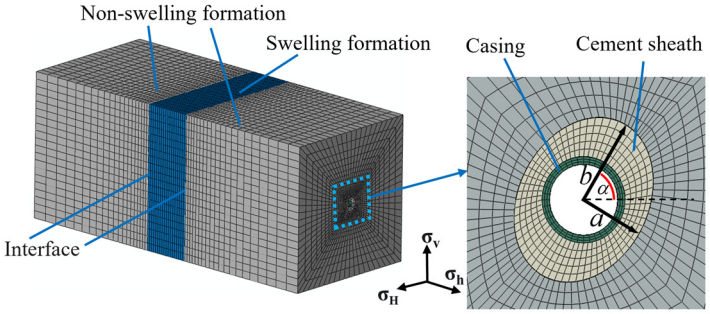

Fig 10. Model of elliptical cement sheath

Figure 11 illustrates the effect of cement sheath ellipticity on casing stress when the shale swelling percentage is 0.4% and the azimuth angle is 30°. For all cement sheath ellipticities, the zones of maximum stress on the casing inner wall consistently occur in the horizontal direction, which is consistent with the stress distribution characteristics of a casing subjected to compressive loading. As the cement sheath ellipticity increases, the yielded regions expand on the casing outer wall in the σ_v direction and on the inner wall in the σ_H direction, leading to intensified stress concentration and progressively aggravated casing ovalization. When the cement sheath ellipticity reaches 1.4, pronounced plastic deformation develops on both the inner and outer walls of the casing, indicating a significantly reduced resistance to shale-induced compressive loading. This response is primarily attributed to the non-uniform stress transfer caused by the elliptical geometry of the cement sheath. As can be seen from the Figure 12, with the increase of the azimuth of the major axis of the ellipse, the yield areas of the outer wall in the σ_v direction and the inner wall in the σ_H direction of the inner wall of the casing decrease. This behavior can be explained by the fact that shale swelling predominantly develops in the σ_v direction, while the cement sheath has a larger wall thickness in the σ_H direction, which resists the elliptical deformation of the casing. Moreover, when the major axis of the elliptical cement sheath is oriented at 0° or 90°, the casing stress exhibits a symmetric distribution. In contrast, at azimuthal angles of 30° and 60°, the stress concentration region on the casing shows a noticeable deviation. This behavior arises because variations in the orientation of the elliptical cement sheath alter the symmetry of stress transmission paths.

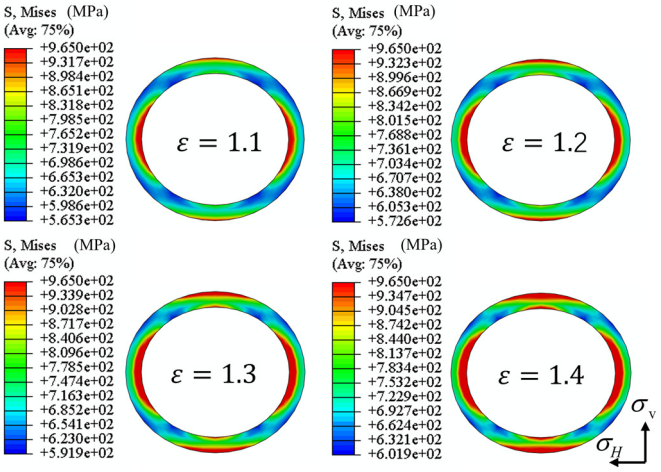

Fig 11. Contour plots of casing stress with different cement sheath ellipticities

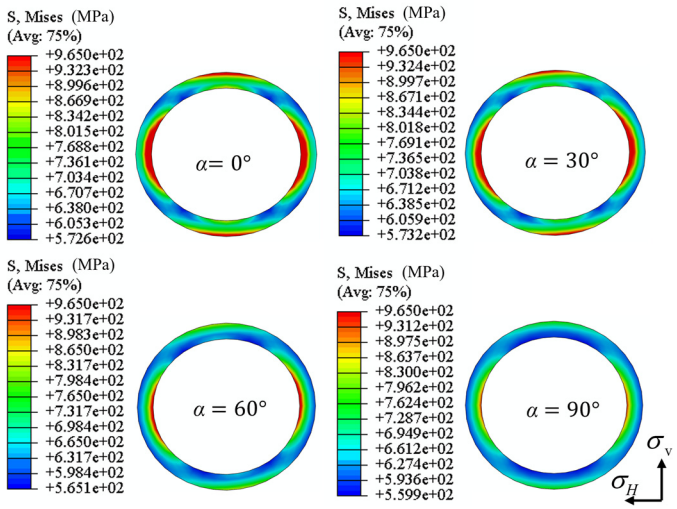

Fig 12. Contour plots of casing stress with different orientations of elliptical cement sheaths

Figure 13 presents the casing inner diameter under the combined effects of shale swelling and an elliptical cement sheath. As shown in Fig. 13(a), under vertical compression induced by shale swelling, casing ovalization becomes more pronounced with increasing cement sheath ellipticity. Therefore, in swelling shale intervals, an elliptical cement sheath significantly aggravates casing deformation. Figure 13(b) also indicates that casing ovalization decreases with increasing azimuth angle of the cement sheath. When the orientation of the elliptical cement sheath coincides with either the maximum horizontal or vertical in-situ stress direction, stress transmission is symmetric, resulting in a symmetric stress distribution along the casing inner wall. In contrast, when the cement sheath is oriented in other directions, asymmetric stress transfer paths caused by shale compression lead to a slight rotation of the casing stress concentration. This finding explains the non-uniform orientations of casing ovalization observed in logging data. Consequently, improving wellbore integrity is essential to suppress post-cementing cement sheath ellipticity, for example, by enhancing borehole stability through optimized drilling fluid performance or by reducing drill string vibration during drilling operations.

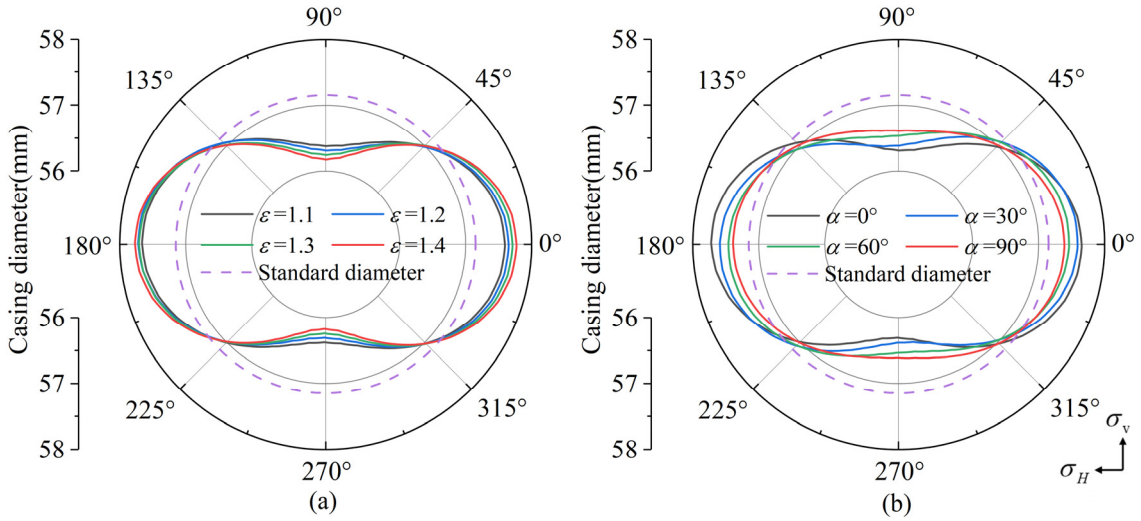

Fig 13. Casing inner diameter under cement sheaths with different elliptical characteristics:(a) Cement sheath ellipticity; (b) Orientation of the major axis of the elliptical cement sheath

4.2.2. Combined Influence of Shale Swelling and Cement Sheath Void on Casing Deformation

To investigate the combined effects of shale swelling and cement sheath voids on casing deformation, the model shown in Figure 14 was employed to simulate casing stress under cement sheath void angles ranging from 0° to 120°, where θ denotes the void angle and α represents the void azimuth. In addition, with the void angle fixed at 30° and the shale swelling percentage set to 0.4%, casing stress distributions were calculated for void azimuths of 0°, 30°, 60°, and 90° to evaluate the influence of void orientation on casing deformation in shale gas wells.

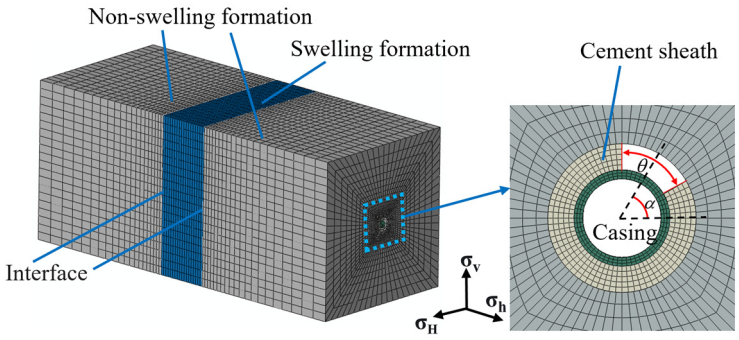

Fig 14. Model of cement sheath void

Figure 15 shows the casing stress distribution under different cement sheath void angles at a shale swelling percentage of 0.4% and a void azimuth of 0°. When the void angle is 30°, casing yielding is concentrated within the cement sheath void region, with additional yielding observed on both sides of the void. As the void angle increases, the yielding zones at the void and its adjacent sides expand progressively, while yielding also develops on the opposite side of the casing. Figure 16 illustrates the casing stress distribution under different void azimuths at a shale swelling percentage of 0.4% and a void angle of 30°. As the void azimuth increases toward 90°, the yielding region remains localized near the void, and the overall yielding area gradually decreases.

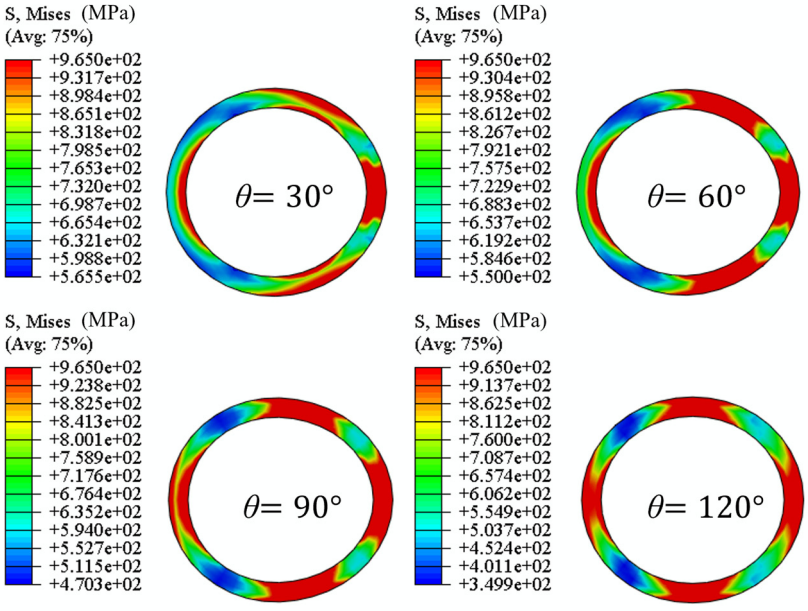

Fig 15. Contour plots of casing stress at different cement sheath void angles

Figure 17(a) presents the post-deformation inner diameter of the casing under different cement sheath void angles. With increasing void angle, the degree of ovalization induced by compressive loading is intensified. In addition, a larger void angle causes an overall displacement of the casing toward the void region, as the casing loses external support from the cement sheath under the combined action of internal pressure and shale compression in the σ_v direction. Figure 17(b) illustrates the casing inner diameter after deformation for different void azimuths. As the void azimuth increases from 0° to 90°,

casing deformation gradually diminishes, and the direction of outward bulging shifts accordingly, while remaining adjacent to the void region. This behavior arises because shale swelling predominantly occurs in the σ_v direction.

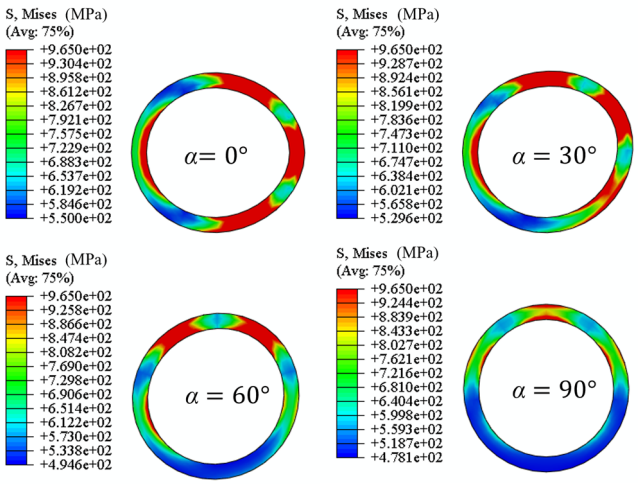

Fig 16. Contour plots of casing stress at different cement sheath void azimuth

As the void approaches the σ_v direction, the absence of the cement sheath provides deformation space for the swelling shale, thereby reducing stress transfer to the casing. Overall, at a given shale swelling percentage, cement sheath voids significantly exacerbate casing deformation, while the relative orientation between the void azimuth and shale bedding direction further influences deformation severity. Therefore, improving cement sheath integrity is essential to mitigate deformation risks. This can be achieved by enhancing slurry displacement efficiency in clay-rich intervals and near perforation clusters during cementing, as well as optimizing hydraulic fracturing parameters to avoid disturbance-induced cement sheath damage.

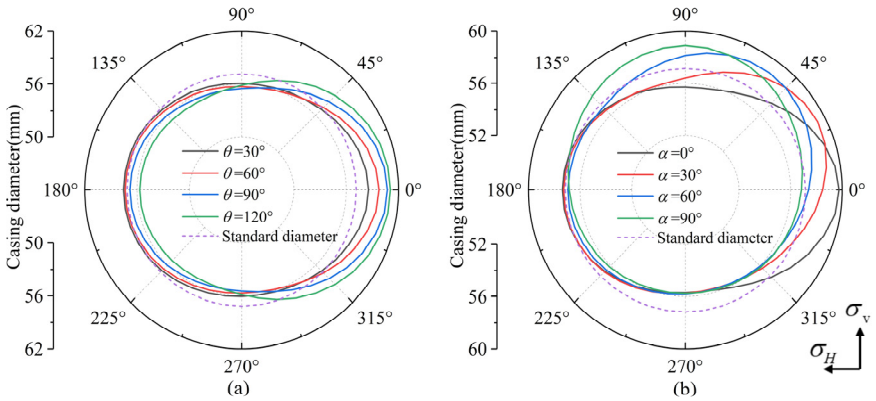

Fig 17. Casing inner diameter under different cement sheath void characteristics:(a) Cement sheath void angle; (b) Cement sheath void orientation

5. CONCLUSION

This study investigated casing deformation during hydraulic fracturing in horizontal wells in southern Sichuan. Based on regional deformation characteristics, finite element models were developed to elucidate the differential effects of shale swelling on casing stress distribution, as well as the combined influence of shale swelling and cementing quality on casing deformation. The following conclusions can be drawn from the analysis.

Shale swelling induced by fluid–rock hydration reactions is identified as the primary cause of casing deformation in the study area. With increasing shale swelling percentage, casing stress rises

progressively, and once the yield strength is exceeded, oval deformation occurs. As the extent of the hydrated zone increases, casing diameter reduction increases initially and then gradually stabilizes, with the shrinkage in the central swelling zone approaching a steady value.

Cementing quality in hydrated shale intervals exerts a non-negligible influence on casing integrity. Cement sheath voids and ellipticity significantly affect casing stress distribution. Greater cement sheath ellipticity results in a wider yielding region and more severe deformation, while increasing void angles lead to enlarged yielding areas and intensified casing deformation. In addition, the severity of casing deformation is strongly controlled by the azimuth of cementing defects and its alignment with the shale swelling direction.

From an engineering perspective, shale swelling during hydraulic fracturing should be mitigated by optimizing fracturing fluid formulations, such as incorporating clay stabilizers or using high-viscosity fluids. Improvements in drilling fluid performance and control of drill string vibration are also recommended to enhance wellbore stability and prevent irregular cement sheath thickness caused by borehole damage. Furthermore, cementing operations should prioritize displacement efficiency in clay-rich intervals and near perforation clusters to ensure cement sheath integrity, thereby reducing stress concentration and the risk of casing failure.

DISCLOSURE STATEMENT

The authors have no financial or proprietary interests in any material discussed in this article.

REFERENCES

[1] Zhao, L., X. Qin, J. Zhang, X. Liu, D. Han, J. Geng, and Y. Xiong. 2018. An Effective Reservoir Parameter for Seismic Characterization of Organic Shale Reservoir. Surveys in Geophysics 39(3): 509–541. doi: 10.1007/s10712-017-9456-9.

[2] Ma, X., and J. Xie. 2018. The Progress and Prospects of Shale Gas Exploration and Development in Southern Sichuan Basin, SW China. Petroleum Exploration and Development 45(1): 172–182. doi: 10.1016/s1876-3804(18) 30018-1.

[3] Yin, A., J. Li, W. Lian, and H. Zhang. 2025. Research progress on the mechanisms and control methods of casing deformation in shale gas horizontal wells. Xinjiang Oil & Gas 21(01):50-60. doi: 10.12388/j.issn.1673-2677.2025. 01. 006.

[4] Dong, K., N. Liu, Z. Chen, R. Huang, J. Ding, and G. Niu. 2019. Geomechanical analysis on casing deformation in Longmaxi shale formation. Journal of Petroleum Science and Engineering, 177: 724–733. doi: 10.1016/j.petrol. 2019. 02.068.

[5] Zhang, P., Y. He, Z. Liu, H. Tong, C. Deng, X. Ren, H. Zhang, et al. 2021. Shear Compression Deformation Test and Deformation Prevention Practice of Casing in Shale Gas Horizontal Wells. Natural Gas Industry B 8(5): 514–522. doi: 10.1016/j.ngib.2021.08.008.

[6] Guo, X., Li, J., Liu, G., Xi, Y., Zeng, Y., He, M., and Yan, H. (2019). Numerical simulation of casing deformation during volume fracturing of horizontal shale gas wells. Journal of Petroleum Science and Engineering, 172, 731–742. doi: 10.1016/j.petrol.2018.08.067.

[7] Yin, F., L. Han, S. Yang, Y. Deng, Y. He, and X. Wu. 2018. Casing deformation from fracture slip in hydraulic fracturing. Journal of Petroleum Science and Engineering 166: 235-241. doi: 10.1016/j.petrol.2018.03.010.

[8] Zhang, F., Z. Jiang, Z. Chen, Z. Yin, and J. Tang. 2020. Hydraulic Fracturing Induced Fault Slip and Casing Shear in Sichuan Basin: A Multi-Scale Numerical Investigation. Journal of Petroleum Science and Engineering 195: 107797. doi: 10.1016/j.petrol.2020.107797.

[9] Yan, W., L. Zou, H. Li, J. Deng, H. Ge, and H. Wang. 2017. Investigation of Casing Deformation during Hydraulic Fracturing in High Geo-Stress Shale Gas Play. Journal of Petroleum Science and Engineering 150: 22–29. doi: 10.1016/j.petrol.2016.11.007.

[10] Xi, Y., J. Li, G. Liu, C. Cha, and Y. Fu. 2018. Numerical Investigation for Different Casing Deformation Reasons in Weiyuan-Changning Shale Gas Field during Multistage Hydraulic Fracturing. Journal of Petroleum Science and Engineering 163: 691–702. doi: 10.1016/j.petrol.2017.11.020.

[11] Lian, Z., Yu, H., Lin, T., & Guo, J. 2015. A study on casing deformation failure during multi-stage hydraulic fracturing for the stimulated reservoir volume of horizontal shale wells. Journal of Natural Gas Science and Engineering, 23, 538-546. doi: 10.1016/j.jngse.2015.02.028

[12] Yu, H., Lian, Z., & Lin, T. 2014. Finite element analysis of failure mechanism of casing during shale gas fracturing. China Petroleum Machinery, 42(8), 84-88.

[13] Zhang, X., J. Liu, W. Cheng, W. Jiang, J. Jin, and L. Shen. 2022. New Type of Casing Deformation Rising in Weiyuan Changning Shale Gas Play. In International Petroleum Technology Conference. Riyadh, Saudi Arabia: IPTC. doi: 10.2523/iptc-22679-ea.

[14] Liu, K., D. Gao, Y. Wang, and Y. Liu. 2016. Effects of local load on shale gas well casing deformation. Nat. Gas Ind 36: 76-82. doi: 10.3787/j.issn.1000-0976.2016.11.010.

[15] Yin, F., B. Shi, G. Huang, and X. Wu. 2023. Integrity Assessment Methodology of Casing Ovality Deformation in Shale Gas Wells. Geoenergy Science and Engineering 224: 211643. doi: 10.1016/j.geoen.2023.211643.

[16] Skomedal, E., J. Park, D.V. Huynh, and J.C. Choi. 2019. Formation Induced Well Deformation. In SPE Europec Featured at 81st EAGE Conference and Exhibition. London, England, UK: SPE. doi: 10.2118/195475-ms.

[17] Liu, X., W. Zeng, L. Liang, and J. Xiong. 2016. Experimental Study on Hydration Damage Mechanism of Shale from the Longmaxi Formation in Southern Sichuan Basin, China. Petroleum 2(1): 54–60. doi: 10.1016/j. petlm. 2016.01.002.

[18] Wang, Y., X. Liu, L. Liang, and J. Xiong. 2020. Experimental Study on the Damage of Organic-Rich Shale during Water-Shale Interaction. Journal of Natural Gas Science and Engineering 74: 103103. doi: 10.1016/j.jngse. 2019. 103103.

[19] LI, G., Z. LI, S. HU, M. LI, and Z. LI. 2024. Shale-liquid interaction and its effect on in-situ stress. Journal of Southwest Petroleum University (Science & Technology Edition), 46(05): 115-123. doi: 10.11885/j.issn.1674-5086.2022.06.29.01.

[20] Gao, S., Z. Hu, W. Guo, L. Zuo, and R. Shen. 2013. Water absorption characteristics of gas shale and the fracturing fluid flowback capacity. Nat. Gas Ind, 33(12): 71-76. doi:10.3787/j.issn.1000-0976.2013.12.010.

[21] Meng, M., H. Ge, Y. Shen, Q. Hu, L. Li, Z. Gao, T. Tian, and J. Chao. 2020. The Effect of Clay-Swelling Induced Cracks on Imbibition Behavior of Marine Shale Reservoirs. Journal of Natural Gas Science and Engineering 83: 103525. doi: 10.1016/j.jngse.2020.103525.

[22] Li, G., Z. Li, and Z. Jiang, H. Yu, L. He. 2021. A study on the effect of shale-liquid reaction on casing deformation. Journal of Southwest Petroleum University (Natural Science Edition) 43(01): 103-10. doi: 10.11885/j.issn.1674-5086.2019.12.23.01.

[23] Zhang, R., B. Zhang, L. Cao, N. Lu, Y. Xu, L. Wu, S. Wang, and R. Jiang. 2024. Evaluation of the Casing Strength Reliability in Deep Gas Well by Taking into Account the Cement Quality and Strength Uncertainty: Method, Analysis and Application. Geoenergy Science and Engineering 234: 212623. doi: 10.1016/j.geoen.2023.212623.

[24] Zhu, M., N. Liu, X. Chen, Y. Zou, G. Li, Z. Zhang, and R. Wang. 2024. Numerical Analysis for Mechanical Integrity of Oval Shape Wellbore in Creep Formation. In 58th U.S. Rock Mechanics/Geomechanics Symposium. Golden, Colorado, USA: ARMA. doi: 10.56952/arma-2024-0335.

[25] Gu, C., X. Li, Y. Feng, J. Deng, and K. Gray. 2022. Numerical Investigation of Cement Interface Debonding in Deviated Shale Gas Wells Considering Casing Eccentricity and Residual Drilling Fluid. International Journal of Rock Mechanics and Mining Sciences 158: 105197. doi: 10.1016/j.ijrmms.2022.105197.

[26] Li, Z., G. Li, H. Li, J. Liu, Z. Jiang, and F. (Bill) Zeng. 2023. Effects of Shale Swelling on Shale Mechanics during Shale–Liquid Interaction. Energy 279: 128098. doi: 10.1016/j.energy.2023.128098.

[27] Li, G., Z. Li, and Z. Jiang, H. Yu, L. He. 2021. Study on the Mechanism of Shale Expansion on Casing Deformation in Weirong Field. Chinese Journal of Underground Space and Engineering 17(6): 2007-2014. doi:10.3969/j. issn. 1673-0836.2021.6. dxkj202106038.

[28] Li, H., Z. Li, G. Li, H. Yu, Z. Jiang, L. He, B. Guo, and M. Dong. 2020. Casing deformation mechanisms of horizontal wells in Weirong shale gas field during multistage hydraulic fracturing. Journal of Natural Gas Science and Engineering 84: 103646. doi: 10.1016/j.jngse.2020.103646.

[29] Teng, X., M. Chen, Y. Jin, Y. Lu, & Y. Xia. 2017. Poroelastic dynamics mechanisms of wellbore instability in tight formations. Petroleum Science Bulletin, 2(4), 478-489.

[30] Mises, R. V. (1913). Mechanik der festen Körper im plastisch-deformablen Zustand. Nachrichten von der Gesellschaft der Wissenschaften zu Göttingen, Mathematisch-Physikalische Klasse, 1913, 582-592.

[31] Liu, H., H. Sun, S. Cui, S. Wang, and S. Du. 2023. Study on the deformation mechanism and mechanical properties of bedding shale. Chinese Journal of Underground Space and Engineering 19: 174-180.